

# Surface Modification of Magnesium Ferrite Nanoparticles for Selective and Sustainable Remediation of Congo Red

Supawitch Hoiyang, Tanapong Kunakham, Jeeranan Nonkumwong, Kajornsak Faungnawakij, Supon Ananta, Piyarat Nimmanpipug, T. Randall Lee, and Laongnuan Srisombat\*



Cite This: *ACS Appl. Nano Mater.* 2021, 4, 10244–10256



Read Online

ACCESS |



Metrics & More



Article Recommendations



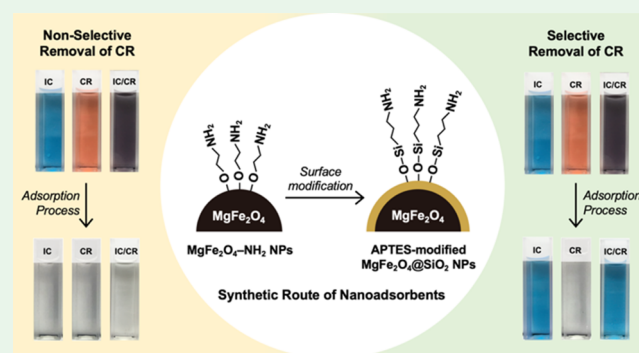
Supporting Information

**ABSTRACT:** Surface modification of silica-coated magnesium ferrite nanoparticles ( $\text{MgFe}_2\text{O}_4@SiO_2$  NPs) by 3-aminopropyltriethoxysilane (APTES) shows enhanced selectivity for the removal of Congo Red (CR) from both single and binary aqueous dye solutions. Before coating the surfaces of amine-functionalized magnesium ferrite nanoparticles ( $\text{MgFe}_2\text{O}_4\text{-NH}_2$  NPs) with silica, control studies of the adsorption of cationic, neutral, and anionic dyes were performed using both single and binary dye systems. The studies found that the  $\text{MgFe}_2\text{O}_4\text{-NH}_2$  nanoadsorbent favors the adsorption of indigo carmine (IC) and CR in single dye solutions (>90% removal efficiencies). However,  $\text{MgFe}_2\text{O}_4\text{-NH}_2$  NPs preferentially adsorb CR in binary dye solutions. Interestingly, the selectivity of CR over IC depends on the initial concentration of IC/CR in the IC/CR binary systems. A further enhancement in the selective removal of CR in both single and binary dye solutions was achieved by coating the  $\text{MgFe}_2\text{O}_4\text{-NH}_2$  NPs with silica followed by modification with APTES (i.e., APTES-modified  $\text{MgFe}_2\text{O}_4@SiO_2$  NPs). The highly selective adsorption capacity for CR on the APTES-modified  $\text{MgFe}_2\text{O}_4@SiO_2$  nanoadsorbent was attributed to the mixture of polar functional groups (i.e.,  $-\text{OH}$  and  $-\text{NH}_2$ ) on the surface of the nanoadsorbent, which facilitates adsorbent–adsorbate interactions such as electrostatic and hydrogen-bonding interactions, which are amplified for CR with its more numerous polar functional groups (i.e., amine, azo, and sulfonate groups). From the results, the APTES-modified  $\text{MgFe}_2\text{O}_4@SiO_2$  nanoadsorbent offers an effective, inexpensive, and reusable/sustainable system for the selective removal and remediation of Congo Red from wastewaters.

**KEYWORDS:** magnesium ferrite nanoparticles, surface modification, amine-functionalized magnetic nanoparticles, nanoadsorbent, selective dye removal, Congo Red

## 1. INTRODUCTION

Water pollution has been an ongoing societal concern due to continuing worldwide industrial growth.<sup>1,2</sup> Industries involving coloring, such as textile, leather, and printing, are of particular concern as dyes are major pollutants of wastewater.<sup>3</sup> The abundant amounts of dyes in effluents are harmful to both organisms and humans. In addition to their high toxicity and resistance to biodegradation, the dyes are often mutagenic and can cause cancer in humans.<sup>4,5</sup> To reduce water pollution, it is necessary to remove or recover the contaminated dye in wastewater before returning the water to natural resources. Among various approaches for dye removal, adsorption has received much attention due to its high performance, simplicity of operation, and ready availability of several adsorbents.<sup>3</sup> Numerous studies have explored the use of magnetic nanomaterials, especially ferrite-based nanoparticles, as efficient adsorbents.<sup>6–9</sup> These materials not only provide the ability to remove various contaminants but also are easily separated from the treated solution after the adsorption



process using an external magnet,<sup>7</sup> thereby providing a pathway toward a reusable and sustainable remediation technique. Among ferrite-based nanoparticles, magnesium ferrite suits to use as an alternative adsorbent since it is a superparamagnetic and noncytotoxic material that offers both practical usage and environmental safety.<sup>10</sup>

Selectivity is one of the most important factors when choosing a good adsorbent. An adsorbent with high selectivity for removal of the targeted dyes can be utilized to recover the targeted molecule and/or to serve as a sensor for the detection and identification of certain types of dyes.<sup>11,12</sup> However, the design of adsorbents with binding abilities to specific molecules

Received: July 1, 2021

Accepted: August 24, 2021

Published: September 25, 2021

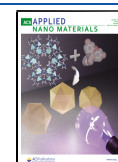
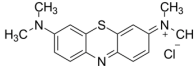
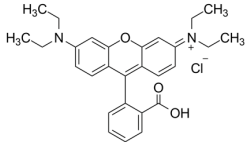
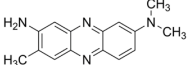
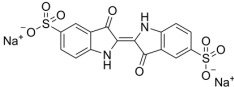
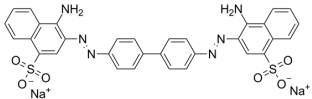
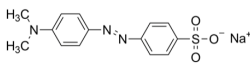


Table 1. Chemical Forms and Maximum Absorption Wavelengths ( $\lambda_{\max}$ ) of the Used Dyes<sup>a</sup>

Dye classification	Dye	Chemical structure	$\lambda_{\max}$ (nm)
Cationic dye	MB		664
	RhB		554
Neutral dye	NR		462
Anionic dye	IC		611
	CR		499
	MO		464

<sup>a</sup>These  $\lambda_{\max}$  values were estimated at pH  $\sim$ 7.

is challenging since there are several factors influencing selectivity. For example, the surface charge of the adsorbent directly affects the selectivity of dye adsorption. Qin et al. reported that quaternary amine-functionalized polymers showed selective removal of anionic dyes.<sup>13</sup> Likewise, Chen and co-workers fabricated secondary amine-functionalized silica for the selective adsorption of anionic dyes.<sup>14</sup> The existence of amine-based functional groups on the surfaces of these adsorbents provides positive charges that are suitable for attractive electrostatic interactions with anionic molecules. Therefore, surface modification stands as an attractive strategy to design adsorbents with high selectivity for targeted dye removal.

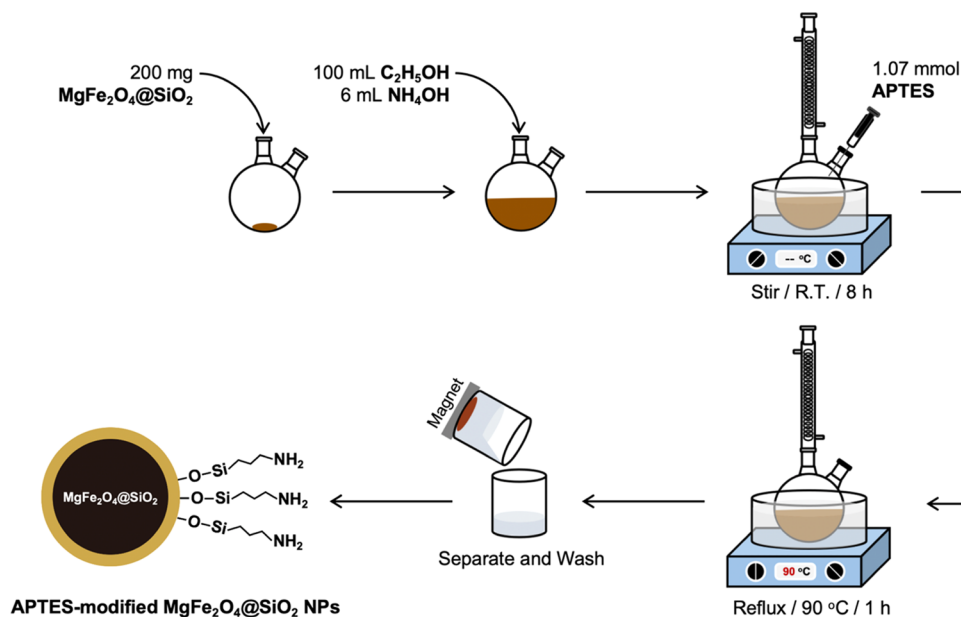
In recent years, surface-functionalized magnesium ferrite nanoparticles ( $\text{MgFe}_2\text{O}_4$  NPs) have been fabricated by our research group.<sup>15–17</sup> Perhaps the most interesting materials are the amine-functionalized  $\text{MgFe}_2\text{O}_4$  NPs ( $\text{MgFe}_2\text{O}_4\text{-NH}_2$ ) in which ethanolamine is used as a surface modifier.  $\text{MgFe}_2\text{O}_4\text{-NH}_2$  NPs can be utilized as efficient adsorbents for the removal of hazardous substances, such as heavy metal ions like Pb(II) and anionic dyes like Congo Red.<sup>15,16</sup> High removal efficiencies (>90%) for these contaminants of  $\text{MgFe}_2\text{O}_4\text{-NH}_2$  NPs were obtained. Interestingly, with regard to selectivity,  $\text{MgFe}_2\text{O}_4\text{-NH}_2$  NPs provided high selectivity for Pb(II) adsorption in binary solutions containing Pb(II) and various metal ions such as Ca(II), Cd(II), Zn(II), Cu(II), and Ni(II) ions.<sup>15</sup> With regard to dye removal, except for CR adsorption, the adsorption behavior of  $\text{MgFe}_2\text{O}_4\text{-NH}_2$  NPs toward other dyes has not been examined. As such, the specificity of dye removal by these nanoadsorbents has yet to be determined.

In this study, the adsorption behaviors of several dyes by  $\text{MgFe}_2\text{O}_4\text{-NH}_2$  NPs were systematically investigated. Different types of dyes (i.e., cationic, neutral, and anionic dyes) were

used as model contaminants in single-component systems to evaluate the ability to adsorb each type of dye under various initial pH values of a dye solution. In addition to single-component dye solutions, the adsorption behaviors of dyes in binary solutions with either different (e.g., cationic vs anionic) or similar (e.g., anionic vs anionic) types of dyes were also examined with the goal toward selective adsorption of CR. However, when examining the removal of anionic dyes, the  $\text{MgFe}_2\text{O}_4\text{-NH}_2$  NPs provided efficient adsorption of both CR and anionic indigo carmine (IC) even in binary IC/CR mixtures, indicating that the  $\text{MgFe}_2\text{O}_4\text{-NH}_2$  NPs lack high selectivity for CR removal. To address this shortcoming, we encapsulated the  $\text{MgFe}_2\text{O}_4\text{-NH}_2$  NPs within a thin silica shell followed by amino functionalization (3-aminopropyltriethoxysilane, APTES) on the silica surface to increase the selectivity for CR. APTES was used as a surface modifier since not only it provides structural stability and inertness to redox reactions of the magnetic nanoadsorbent but also provides an amine group on the surfaces of the modified adsorbents, which offers the linking of a specific adsorbate.<sup>18,19</sup> Several characterization techniques (i.e., X-ray diffraction (XRD), Fourier transform infrared (FTIR) spectroscopy, X-ray photoelectron spectroscopy (XPS), scanning electron microscopy (SEM), and  $\zeta$ -potential analysis) were employed to characterize the modified nanoadsorbent. The adsorption behavior of anionic dyes, in particular IC and CR, in both single and binary systems was examined using the as-modified nanoparticles.

## 2. EXPERIMENTAL SECTION

**2.1. Materials.** The amine-functionalized magnesium ferrite nanoparticles ( $\text{MgFe}_2\text{O}_4\text{-NH}_2$  NPs) were synthesized by following our previous work, wherein details of the preparation method and characterization are fully provided.<sup>15,16</sup> The synthesis of  $\text{MgFe}_2\text{O}_4\text{-NH}_2$  NPs is given in the Supporting Information. Reagent-grade

Scheme 1. Surface Functionalization of MgFe<sub>2</sub>O<sub>4</sub>@SiO<sub>2</sub> NPs by APTES

samples of the representative dyes Congo Red (CR, Loba Chemie), indigo carmine (IC, Merck), methyl orange (MO, KemAUS), methylene blue (MB, Merck), rhodamine B (RhB, Loba Chemie), and neutral red (NR, Sigma-Aldrich) were used as model contaminants. The chemical structures and the maximum absorption wavelength ( $\lambda_{\max}$ ) of these dyes are listed in Table 1. Absolute ethanol (C<sub>2</sub>H<sub>5</sub>OH, Labsan), 25–28% ammonia solution (NH<sub>4</sub>OH, Merck), and 3-aminopropyltriethoxysilane (APTES, Sigma-Aldrich) were used in the surface-modification process.

## 2.2. Selective Adsorption of Dyes by MgFe<sub>2</sub>O<sub>4</sub>-NH<sub>2</sub> NPs.

**2.2.1. Selectivity Test for Dye Removal in Single-Component Dye Systems.** To explore the selectivity of the MgFe<sub>2</sub>O<sub>4</sub>-NH<sub>2</sub> nano-adsorbent, single and binary systems of dyes were used as model contaminants. The single-component systems were composed of 10 mg L<sup>-1</sup> individual dyes: IC, CR, MO, NR, MB, and RhB. Various initial pH values of the dye solutions (i.e., 3–11) were studied in these systems by adjusting the pH of the solution using 0.1 mol L<sup>-1</sup> nitric acid and 0.1 mol L<sup>-1</sup> sodium hydroxide. Batch adsorption experiments were performed in triplicate. In the studies, 15 mL of dye solution was mixed with 2.8 g L<sup>-1</sup> MgFe<sub>2</sub>O<sub>4</sub>-NH<sub>2</sub> NPs and then shaken using a shaking water bath (Mettmert, WB22/SV1422) at ~30 °C for 4 h. Afterward, the nano-adsorbent was separated from the dye solution by an external magnet. Absorption spectra of the solutions were collected using a UV-vis spectrophotometer (PG Instruments, T80) to determine the amount of dye in the solution for calculating the removal efficiency and adsorption capacity ( $q_e$ ) using eqs 1 and 2, respectively.

$$\text{removal efficiency (\%)} = [(C_0 - C_e)/C_0] \times 100 \quad (1)$$

$$q_e (\text{mg g}^{-1}) = [(C_0 - C_e)/W] \times V \quad (2)$$

where  $C_0$  and  $C_e$  are the dye concentration at initial and equilibrium states (mg L<sup>-1</sup>) and  $V$  and  $W$  are the volume of the dye solution (L) and dry weight of the nano-adsorbent (g), respectively. For the single-component dye systems,  $C_0$  and  $C_e$  of each dye were estimated using a standard calibration curve.

**2.2.2. Selectivity Test for Dye Removal in Binary Dye Systems.** The binary systems were composed of three sets of two mixed dyes: anionic/cationic (IC/RhB and CR/RhB), anionic/neutral (IC/NR), and anionic/anionic (IC/MO, CR/MO, and IC/CR). The batch adsorption experiments were performed similar to those described in Section 2.2.1, except the mixed solution contained 10 mg L<sup>-1</sup> each dye component and the initial pH value of all mixed dye solution was

~7. For the binary system, the removal efficiency and  $q_e$  were calculated using eqs 1 and 2, respectively. The  $C_0$  and  $C_e$  of each dye in the mixture were determined using the linear equations in two variables applied from Beer's law for a multicomponent system<sup>20</sup> as expressed in eqs 3 and 4

$$\text{at } \lambda_1: A_1 = \varepsilon_X^1 b C_X + \varepsilon_Y^1 b C_Y \quad (3)$$

$$\text{at } \lambda_2: A_2 = \varepsilon_X^2 b C_X + \varepsilon_Y^2 b C_Y \quad (4)$$

where  $A_1$  and  $A_2$  are the total absorbances of the mixtures at wavelengths 1 and 2 with respect to  $\lambda_{\max}$  of dyes X and Y, respectively;  $\varepsilon_X^1$ ,  $\varepsilon_X^2$ , and  $\varepsilon_Y^1$ ,  $\varepsilon_Y^2$  are the values of extinction coefficient for dyes X and Y at wavelengths 1 and 2, respectively;  $C_X$  and  $C_Y$  are the concentrations of dyes X and Y in the binary solutions, respectively; and  $b$  is length of the beam in absorbing media (i.e., width of the cuvette).

**2.2.3. Competitive Adsorption between Congo Red and Indigo Carmine in Binary Systems on MgFe<sub>2</sub>O<sub>4</sub>-NH<sub>2</sub> NPs.** Two sets of IC/CR binary solutions were used. One set of solutions had as a 1:1 ratio of the IC/CR concentration (i.e., 10:10, 50:50, 100:100, 150:150, and 200:200 mg L<sup>-1</sup>). The second set had varied ratios of the IC/CR concentration as 1:1, 1:2, 1:3, 1:4, 4:1, 3:1, and 2:1 (i.e., 50:50, 50:100, 50:150, 50:200, 150:50, and 100:50 mg L<sup>-1</sup>, respectively). The procedure for adsorption experiments was similar to that described in Section 2.2.2.

**2.3. Enhanced Selective Removal of Congo Red by APTES-Modified MgFe<sub>2</sub>O<sub>4</sub>@SiO<sub>2</sub> NPs.** **2.3.1. MgFe<sub>2</sub>O<sub>4</sub>-NH<sub>2</sub> NPs Coated with Silica and Modified with APTES.** This process was conducted via two steps as follows: (i) surface coating by silica to prepare the silica-coated MgFe<sub>2</sub>O<sub>4</sub>-NH<sub>2</sub> NPs (MgFe<sub>2</sub>O<sub>4</sub>@SiO<sub>2</sub> NPs) and (ii) surface functionalization to obtain the amine-functionalized MgFe<sub>2</sub>O<sub>4</sub>@SiO<sub>2</sub> NPs (APTES-modified MgFe<sub>2</sub>O<sub>4</sub>@SiO<sub>2</sub> NPs). The MgFe<sub>2</sub>O<sub>4</sub>@SiO<sub>2</sub> NPs were prepared following the well-known Stöber method, as previously reported in our work.<sup>21</sup> The amine-functionalization method was slightly modified from Kim et al.,<sup>22</sup> as illustrated in Scheme 1. Briefly, 200 mg of the as-obtained MgFe<sub>2</sub>O<sub>4</sub>@SiO<sub>2</sub> powder was mixed with 100 mL of absolute ethanol and 6 mL of ammonia solution. Afterward, 1.07 mmol of APTES was rapidly injected into the mixture, stirred for 8 h, and then refluxed at 90 °C for 1 h. The precipitate was separated from the mixture using an external magnet and washed with ethanol several times. The final product was then dried in an open-air oven at 60 °C overnight.



**2.3.2. Characterization.** The phase formation of the as-synthesized APTES-modified  $\text{MgFe}_2\text{O}_4@/\text{SiO}_2$  NPs was monitored by X-ray diffraction (XRD, Rigaku SmartLab) using  $\text{Cu K}\alpha$  radiation ( $\lambda = 1.5406 \text{ \AA}$ ) with  $0.02^\circ$  scan steps at  $2\theta$  ranging from  $10$  to  $90^\circ$ . The functionalization of these nanoparticles was identified by attenuated total reflectance–Fourier transform infrared spectrometry (ATR–FTIR, Thermo Scientific Nicolet iS50) by varying wavenumbers from  $400$  to  $4000 \text{ cm}^{-1}$  with a resolution of  $4 \text{ cm}^{-1}$ . Their morphologies were explored by field emission scanning electron microscopy (FE-SEM, JEOL JSM-7800F). The surface chemical compositions were also characterized by an X-ray photoelectron spectrometer (XPS, Kratos AXIS Ultra DLD) having a monochromatic  $\text{Al K}\alpha$  X-ray source of  $1486.6 \text{ eV}$ . The  $\text{C 1s}$  peak at  $285.0 \text{ eV}$  was used as an internal standard reference. The  $\zeta$ -potential curve was detected at room temperature using a Zetasizer Nano ZS (Brookhaven ZetaPALS) by adjusting the pH of the solution from  $3$  to  $12$  using  $0.1 \text{ mol L}^{-1}$  hydrochloric acid and  $0.1 \text{ mol L}^{-1}$  sodium hydroxide. The powders were carefully dispersed using  $0.1 \text{ mg mL}^{-1}$  concentrations and then adjusting the ionic strength to  $1 \times 10^{-3} \text{ mol L}^{-1}$  using sodium chloride.

**2.3.3. Selectivity Test for Anionic Dye Removal in Single and Binary Systems.** To demonstrate the selective removal capacity for anionic dyes of the as-synthesized APTES-modified  $\text{MgFe}_2\text{O}_4@/\text{SiO}_2$  NPs, the removal of IC and CR dyes in both single-component and binary systems (IC/CR) was performed by employing the procedure described in Section 2.2.2. However, in this current section, the initial pH and concentration of the dye solutions were kept constant as  $\sim 6$  and  $30 \text{ mg L}^{-1}$ , respectively.

**2.3.4. Reusability Test for CR Removal by APTES-Modified  $\text{MgFe}_2\text{O}_4@/\text{SiO}_2$  NPs.** To examine the reusability of the nano-adsorbent, adsorption–desorption studies were performed. In the first cycle of the adsorption process,  $2.8 \text{ g L}^{-1}$  fresh APTES-modified  $\text{MgFe}_2\text{O}_4@/\text{SiO}_2$  NPs was added to  $15 \text{ mL}$  of  $30 \text{ mg L}^{-1}$  CR solution and then shaken at  $\sim 30^\circ \text{C}$  for  $4 \text{ h}$ . Afterward, the nanoadsorbent was separated from the solution using an external magnet. Absorption spectra of the solutions were collected using a UV–vis spectrophotometer to calculate the removal efficiency for CR. The CR-adsorbed nanoadsorbent was dried in an open-air oven at  $60^\circ \text{C}$  overnight. Then, the first cycle of the desorption process was performed by adding the dried nanoadsorbent to  $15 \text{ mL}$  of absolute ethanol at  $\text{pH} \sim 12$  (i.e., adjusted by  $0.1 \text{ mol L}^{-1}$  sodium hydroxide) for release of the adsorbed CR dye from the nanoadsorbent. After the desorption process, the nanoadsorbent was separated, washed with deionized water, and then dried at  $60^\circ \text{C}$  for  $6 \text{ h}$  for further use in the second adsorption process. In the current study, five adsorption–desorption cycles were conducted for each assay.

### 3. RESULTS AND DISCUSSION

**3.1. Selective Removal of Dyes by  $\text{MgFe}_2\text{O}_4\text{–NH}_2$  NPs.** **3.1.1. Effect of Initial Solution pH on Selective Adsorption in Single-Component Dye Systems.** Three types of representative dyes, i.e., anionic (IC, CR, and MO), cationic (MB and RhB), and neutral (NR) dyes, were used as adsorbates; their molecular structures and ionization states at  $\text{pH} 7$  are shown in Table 1. The adsorption behaviors of these dyes by  $\text{MgFe}_2\text{O}_4\text{–NH}_2$  NPs at the initial pH of dye solution ranging from  $\sim 3$  to  $\sim 11$  are demonstrated in terms of the removal efficiency, as shown in Figure 1. The colors of the solutions and UV–vis spectra for each dye before and after the adsorption processes are provided in Figure S1. Generally, the influence of solution pH on the adsorption system can be rationalized by the adsorbent and adsorbate interactions.<sup>23,24</sup> The charges in the adsorbent surface significantly depend on the solution pH. A net zero charge appears on the adsorbent surface when the solution pH is equal to the pH at the point of zero charge ( $\text{pH}_{\text{PZC}}$ ), estimated from the  $\zeta$ -potential curve. When  $\text{pH} < \text{pH}_{\text{PZC}}$ , the surface is positively charged and

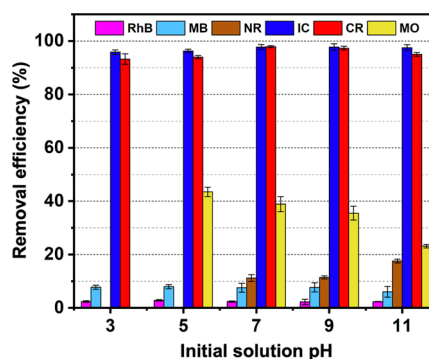


**Figure 1.** Effect of initial solution pH on the removal efficiencies for various dyes of  $\text{MgFe}_2\text{O}_4\text{–NH}_2$  NPs in single-component solution systems.

becomes negative at  $\text{pH} > \text{pH}_{\text{PZC}}$ .<sup>24</sup> In this study, the  $\text{pH}_{\text{PZC}}$  of the  $\text{MgFe}_2\text{O}_4\text{–NH}_2$  NPs is  $\sim 8.4$ .<sup>16</sup> The behavior of the dye contaminant can be influenced by several factors such as charges, the number of binding sites, and so on.<sup>25</sup> In the set of cationic dyes, low removal efficiencies for MB ( $\sim 8\%$ ) and RhB ( $\sim 2\%$ ) are obtained at pH values ranging from  $\sim 3$  to  $\sim 7$  (see Figure 1). Within this pH range, the  $\text{MgFe}_2\text{O}_4\text{–NH}_2$  surface exists as positively charged ( $\text{pH} < 8.4$ ), which leads to strong electrostatic repulsion between the positively charged surface of the adsorbent and the positive charges on the MB and RhB molecules (see the structures in Table 1). Even though the charge on the adsorbent surface can plausibly become negative at  $\text{pH} > 8.4$ , the removal efficiencies for MB and RhB are still quite low. On the whole, the results indicate that the  $\text{MgFe}_2\text{O}_4\text{–NH}_2$  NPs are ineffective for the removal of cationic dyes.

We employed neutral red (NR) as a representative of neutral dyes. However, since NR is a pH indicator, it can exist in two chemical forms (see Figure S2a). Depending on the solution pH, the cationic ( $\text{NRH}^+$ ,  $\text{pH} < 6.8$ ) and neutral (NR,  $\text{pH} > 8.0$ ) forms exhibit red and yellow colors, respectively.<sup>26</sup> The removal efficiencies for NR at  $\text{pH} \sim 3$  and  $\sim 5$  are not reported in this study due to the blue shift in the absorption band during the adsorption processes (see Figure S1c). The removal efficiencies slightly increased from  $\sim 11$  to  $\sim 18\%$  with increasing pH from  $\sim 7$  to  $\sim 11$ , respectively (see Figure 1). At  $\text{pH} \sim 7$ , the dye molecules are likely composed of both  $\text{NRH}^+$  and NR forms, whereas the NR form is solely present at  $\text{pH} \sim 11$ . These observations can be rationalized as follows. First, the repulsion between the positively charged surface of the nanoadsorbent ( $\text{pH} < 8.4$ ) and the  $\text{NRH}^+$  form likely occurs at  $\text{pH} \sim 7$ . Second, the NR form could be adsorbed via other interactions (e.g., hydrogen bonding) rather than electrostatic interactions. Although the removal efficiencies for NR of the  $\text{MgFe}_2\text{O}_4\text{–NH}_2$  NPs are slightly higher than those observed for MB and RhB, low removal efficiencies were still obtained. We therefore conclude that the  $\text{MgFe}_2\text{O}_4\text{–NH}_2$  NPs are not effective for the removal of NR—a conclusion similar to that obtained for the cationic MB and RhB dyes.

High removal efficiencies ( $>90\%$ ) were observed for the anionic IC and CR dyes at pH values ranging from  $\sim 3$  to  $\sim 11$  (see Figure 1). Moreover, no significant changes of the removal efficiencies for IC and CR were revealed, indicating that the adsorption of these dyes was pH-independent. Previously, Regti et al.<sup>27</sup> reported a similar phenomenon involving the pH-independent adsorption of Basic Yellow 28



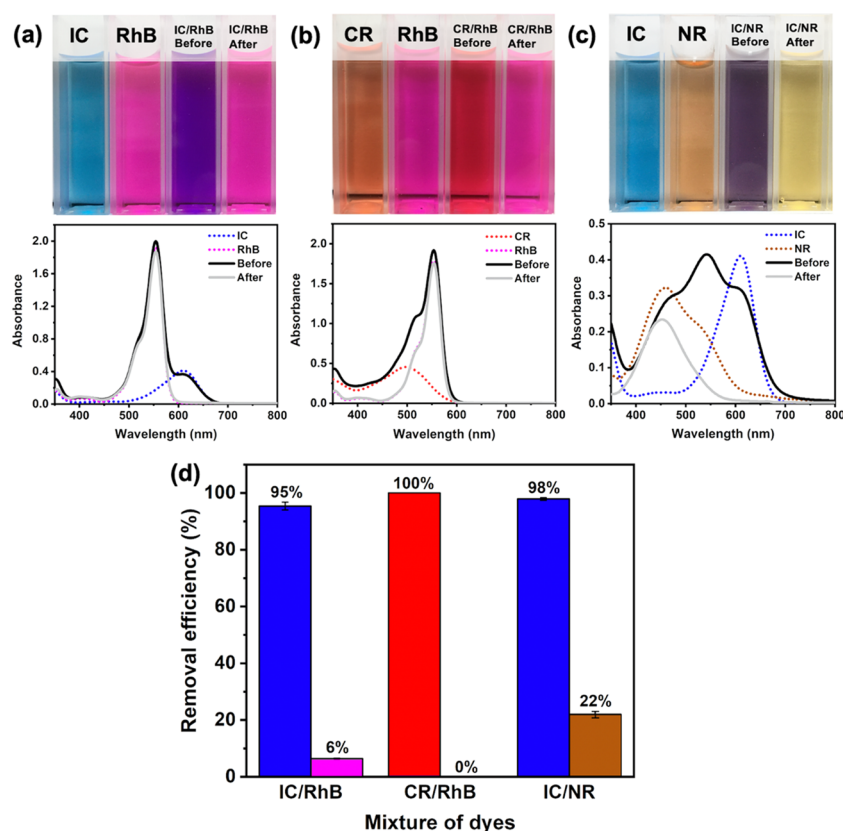


**Figure 2.** (Top) Digital photos and (bottom) UV–vis spectra of anionic/cationic (a) IC/RhB and (b) CR/RhB and (c) anionic/neutral IC/NR binary dye solutions before and after adsorption by  $\text{MgFe}_2\text{O}_4\text{-NH}_2$  NPs. (d) Relative removal efficiencies of dyes in anionic/cationic and anionic/neutral binary dye solutions at pH  $\sim 7$ .

dye by activated carbon. Greater than 90% dye removal efficiencies were obtained at pH values ranging from 2 to 12. In our previous report,<sup>16</sup> we investigated the influence of initial solution pH on CR adsorption by  $\text{MgFe}_2\text{O}_4\text{-NH}_2$  NPs. The results found that the CR removal efficiencies were strongly influenced by the initial pH of the CR solution. With an increase of pH from  $\sim 2$  to  $\sim 6$ , the CR removal efficiencies increased from  $\sim 80$  to  $\sim 96\%$  and then remarkably decreased to lower than 50% at pH  $\sim 12$ . The main adsorption mechanism was then proposed to occur via strong electrostatic attraction between the negative charges of the  $-\text{SO}_3^-$  groups on the CR molecules and the positively charged surface of the adsorbent. In addition to electrostatic interaction, dipole–dipole hydrogen-bonding (between the electronegative amine group of the dye and O atom/surface  $-\text{OH}$  groups of the adsorbent) and Yoshida hydrogen-bonding (between the aromatic ring on the dye molecule and the  $-\text{OH}$  group on the adsorbent surface) interactions could also be involved in the adsorption mechanisms.<sup>28</sup> Compared to our previous report,<sup>16</sup> the only different adsorption parameter is the initial concentration of the dye: in the present study, we used  $10 \text{ mg L}^{-1}$  dye compared to  $30 \text{ mg L}^{-1}$  in the previous study. It is possible that the lower initial concentration of dye could perhaps influence the adsorption mechanism. Moreover, Liu et al.<sup>28</sup> reported that electrostatic interactions were not the predominant factor controlling pH-independent adsorption phenomena. Therefore, we believe that, in this study, other adsorbent–adsorbate interactions (e.g., dipole–dipole hydrogen-bonding and Yoshida hydrogen-bonding interactions) likely play an important role in the adsorption of IC and CR

on  $\text{MgFe}_2\text{O}_4\text{-NH}_2$  NPs due to the slight change of removal efficiencies at all values of the solution pH. Interestingly, this comparison points out that, apart from the effect of initial pH, the initial dye concentration might also be an important factor that influences the adsorption mechanism.

For MO adsorption (see Figure 1), the removal efficiencies noticeably decreased from  $\sim 44$  to  $\sim 23\%$  after tuning the pH from  $\sim 5$  to  $\sim 11$ . However, the removal efficiency at pH  $\sim 3$  is not reported because the protonated form of MO (see Figure S2b) gives rise to a blue shift in the MO absorption band during the adsorption process, as illustrated in Figure S1f. The decrease in MO removal efficiencies as a function of pH can perhaps be attributed to an increase in the negative charge on the adsorbent surface, leading to charge–charge repulsion between the adsorbent and MO molecules at elevated pH values. Interestingly, although MO is an anionic dye similar to IC and CR, a quite low removal efficiency for MO ( $<50\%$ ) was observed. Our result is in agreement with previous studies.<sup>25,29–32</sup> Even though MO is the smallest molecule studied,<sup>33,34</sup> it provides lower removal efficiency. Based on the chemical structures shown in Table 1, MO possesses only one  $-\text{SO}_3^-$  group, while IC and CR possess two  $-\text{SO}_3^-$  groups. IC and CR contain a greater negative charge than MO, leading to stronger binding to the positively charged  $\text{MgFe}_2\text{O}_4\text{-NH}_2$  nano-adsorbent surface.<sup>25,29,31</sup> Additionally, hydrogen bonding plays an important role in IC and CR removal since IC and CR contain primary and secondary amines that offer greater opportunity to form hydrogen bonding with the nano-adsorbent.<sup>28,31,35</sup> Consequently, the  $\text{MgFe}_2\text{O}_4\text{-NH}_2$  nano-adsorbent efficiently removes anionic dyes, particularly IC and

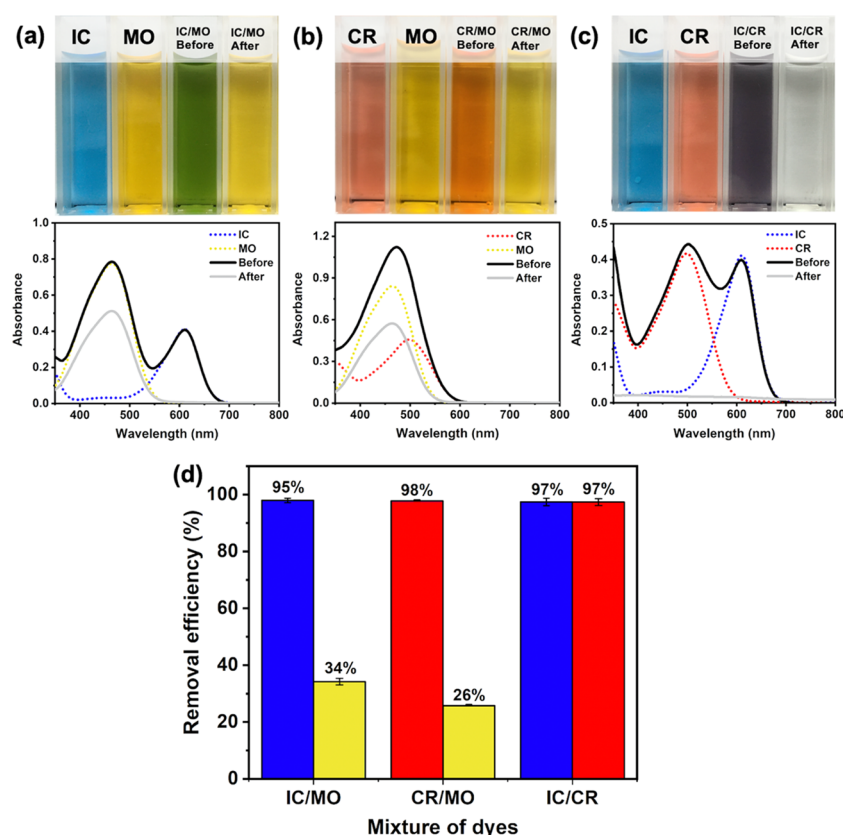


**Figure 3.** (Top) Digital photos and (bottom) UV-vis spectra of anionic/anionic (a) IC/MO, (b) CR/MO, and (c) IC/CR binary dye solutions before and after adsorption by  $\text{MgFe}_2\text{O}_4\text{-NH}_2$  NPs. (d) Relative removal efficiencies for dyes in anionic/anionic binary dye solutions at pH  $\sim 7$ .

CR, in single-component dye systems. Furthermore, the highest removal efficiencies for these dyes are obtained at pH  $\sim 7$ ; we therefore used this pH in all further studies.

**3.1.2. Selectivity of  $\text{MgFe}_2\text{O}_4\text{-NH}_2$  NPs in Binary Dye Systems.** To confirm the inefficient removals of cationic and neutral dyes, the adsorption studies in cationic/cationic (MB/RhB) and cationic/neutral (MB/NR and RhB/NR) binary solutions were investigated. The results indicate unfavored adsorption of cationic and neutral dyes, as shown in Figure S3. To demonstrate the selective removal of anionic dyes by  $\text{MgFe}_2\text{O}_4\text{-NH}_2$  NPs in binary dye solutions, three sets of the solutions, (1) anionic/cationic (IC/RhB and CR/RhB), (2) anionic/neutral (IC/NR), and (3) anionic/anionic (IC/MO, CR/MO, and IC/CR), were used as adsorbates. As illustrated in Figure 2a, the color of the IC/RhB solution changed from purple to fuchsia, which is similar to the color of RhB, after the adsorption process. Correspondingly, the absorption band of IC significantly decreased, while the intensity of the RhB band decreased minimally. These observations indicate that the  $\text{MgFe}_2\text{O}_4\text{-NH}_2$  NPs preferentially remove IC (removal efficiency  $\sim 95\%$ ) in the presence of RhB (removal efficiency  $\sim 6\%$ ) in IC/RhB mixtures. Similarly, the color of the CR/RhB solution changed to fuchsia after the adsorption process (see Figure 2b). Correspondingly, the absorption band of CR significantly decreased, while that of RhB remained unchanged. These observations indicate the preferential removal of CR ( $\sim 100\%$  removal efficiency) over RhB ( $\sim 0\%$  removal efficiency) by the  $\text{MgFe}_2\text{O}_4\text{-NH}_2$  NPs in the CR/RhB solution. In the set of the anionic/neutral binary solution, the color of the IC/NR mixture faded from purple to light yellow (see Figure 2c). The absorption band for CR was not

detectable, whereas the NR band decreased after the adsorption process. Interestingly, the NR removal efficiency in IC/NR binary solutions ( $\sim 22\%$ ) was higher than that of the single-component NR solution ( $\sim 11\%$ , see Figure 1). However, the increase in the NR uptake does not affect the IC adsorption efficiency ( $\sim 98\%$ ) in IC/NR binary solutions. Therefore, the adsorption behaviors of anionic/cationic and anionic/neutral binary solutions by the  $\text{MgFe}_2\text{O}_4\text{-NH}_2$  nanoadsorbent show that the nanoadsorbent exhibits highly selective removal of the anionic dyes IC and CR.

To provide additional evidence for the selective removal of anionic dyes by  $\text{MgFe}_2\text{O}_4\text{-NH}_2$  NPs, the adsorption behaviors of anionic/anionic binary solutions were examined. The results are provided in Figure 3. The color of the IC/MO mixed solution changed from green to yellow after exposure to the nanoadsorbent (see Figure 3a). The absorption band of IC disappeared, while that of MO substantially decreased. Likewise, the color of the CR/MO solution turned yellow, and the overlapping UV-vis absorption band of CR/MO became similar to the characteristic band of MO after the adsorption process (see Figure 3b). The removal efficiencies for IC ( $\sim 95\%$ ) and CR ( $\sim 98\%$ ) in the MO-based binary solutions are high (see Figure 3d) and similar to those in the single-component systems (see Figure 1). Higher removal efficiencies for IC and CR than that for MO are due to stronger electrostatic<sup>25,29,31</sup> and hydrogen-bonding<sup>28,31,35</sup> interactions, as mentioned in Section 3.1.1.

In Figure 3c, the color of IC/CR solution changed from dark purple to colorless after the adsorption process, which is consistent with undetectable IC and CR absorption bands for these experiments. These results demonstrate that IC and CR

dyes were removed by the nanoadsorbent, consistent with the high removal efficiencies for IC (~97%) and CR (~97%). However, high removal efficiencies for IC and CR (almost 100%) in the IC/CR binary solution can be attributed, at least in part, to low initial IC/CR concentrations (i.e., 10:10 mg L<sup>-1</sup>). A previous study found that a high removal efficiency for CR (~96%) was obtained using 30 mg L<sup>-1</sup> initial CR concentration.<sup>16</sup> Similarly, our preliminary studies found an IC removal efficiency of ~96% using 30 mg L<sup>-1</sup> initial IC concentration (data not provided). Therefore, the use of low initial concentrations of IC/CR in binary solutions might be unable to distinguish the adsorption behaviors of IC and CR dyes. With regard to the results in this section, we conclude that the MgFe<sub>2</sub>O<sub>4</sub>-NH<sub>2</sub> nanoadsorbent preferentially adsorbs anionic dyes following the order IC ≈ CR > MO. Importantly, these results led us to recognize the need for further studies on the adsorption behavior of IC/CR binary solutions by MgFe<sub>2</sub>O<sub>4</sub>-NH<sub>2</sub> NPs using higher initial concentrations, which are described in Section 3.1.3.

**3.1.3. Competitive Adsorption between Congo Red and Indigo Carmine on MgFe<sub>2</sub>O<sub>4</sub>-NH<sub>2</sub> NPs.** Two sets of IC/CR binary solutions were used as adsorbates. The first set was fixed as a 1:1 ratio of IC/CR concentrations such as 50:50, 100:100, 150:150, and 200:200 mg L<sup>-1</sup>. Figure 4a shows that the 50:50 mg L<sup>-1</sup> IC/CR solution turned blue after the adsorption process. Similarly, when the initial IC/CR concentration was

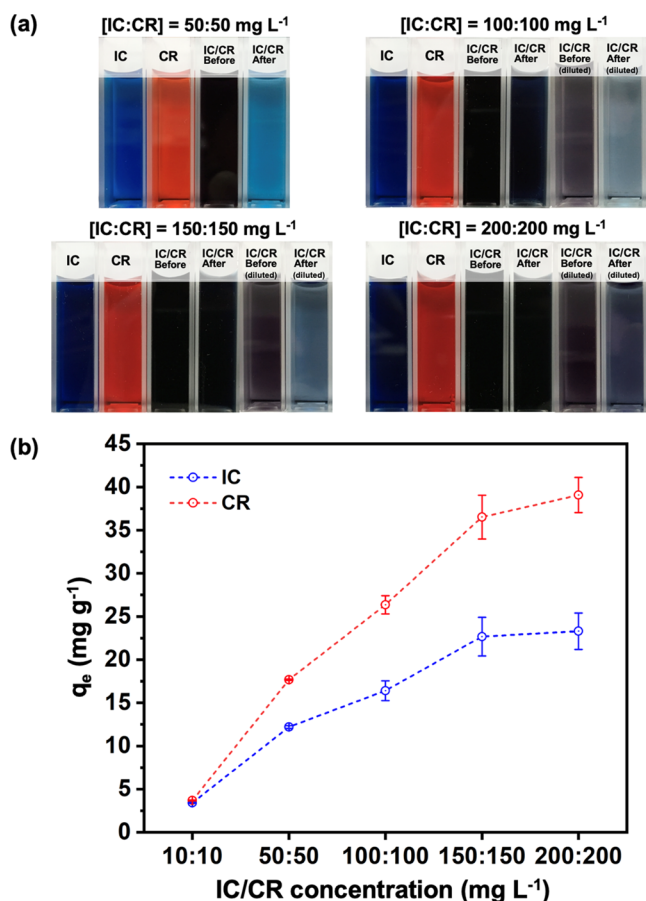


**Figure 4.** (a) Digital photos of IC/CR binary dye solutions before and after adsorption by MgFe<sub>2</sub>O<sub>4</sub>-NH<sub>2</sub> NPs. (b) Adsorption capacities of IC and CR ( $q_e$ ) on MgFe<sub>2</sub>O<sub>4</sub>-NH<sub>2</sub> NPs using a 1:1 ratio of IC/CR concentrations at pH ~7.

increased from 100:100 to 200:200 mg L<sup>-1</sup>, the solutions changed to dark blue after mixing with MgFe<sub>2</sub>O<sub>4</sub>-NH<sub>2</sub> NPs. The adsorption capacities ( $q_e$ ) of IC and CR on the MgFe<sub>2</sub>O<sub>4</sub>-NH<sub>2</sub> nanoadsorbent are provided in Figure 4b. At an IC/CR concentration of 10:10 mg L<sup>-1</sup>, the adsorption capacities of IC and CR are 3.42 and 3.69 mg g<sup>-1</sup>, respectively. With an increase in IC/CR concentrations from 50:50 to 200:200 mg L<sup>-1</sup>, the adsorption capacities of IC and CR increased from 12.2 to 23.3 and 17.1 to 39.1 mg g<sup>-1</sup>, respectively. From the results, the obtained adsorption capacities of CR are higher than those of IC over all ranges of the initial IC/CR concentrations, except for 10:10 mg L<sup>-1</sup>. These results therefore indicate the preferential adsorption of CR in IC/CR binary solutions by MgFe<sub>2</sub>O<sub>4</sub>-NH<sub>2</sub> NPs.

Generally, the molecular selectivity of an adsorbent can be examined using two important parameters: the static distribution coefficient ( $K_D$ , L g<sup>-1</sup>) and the separation factor ( $\alpha$ ) described as follows<sup>28,36</sup>

$$K_D = q_e / C_e \quad (5)$$

where  $q_e$  and  $C_e$  are the amount of adsorbed dye on the adsorbent (mg g<sup>-1</sup>) and the amount of dye remaining in solution (mg L<sup>-1</sup>) at the equilibrium state, respectively. The ratio of two distribution coefficients (i.e.,  $K_{D(X)}$  and  $K_{D(Y)}$ ) can be used to rationalize the selectivity of dye X in the X/Y binary solution expressed as follows

$$\alpha_{X/Y} = K_{D(X)} / K_{D(Y)} \quad (6)$$

Importantly, a value of  $\alpha$  close to 1.0 indicates no selectivity by the proposed adsorbent.

Table 2 shows the partition coefficients and selectivity factors for both IC and CR in the IC/CR binary solutions at

**Table 2.** Molecular Selectivity of MgFe<sub>2</sub>O<sub>4</sub>-NH<sub>2</sub> NPs in the IC/CR Binary Dye Solutions Using a 1:1 Ratio of IC/CR Concentrations at pH ~7

[IC:CR] (mg L <sup>-1</sup> )	$K_D$ (L g <sup>-1</sup> )		$\alpha_{IC/CR}$	$\alpha_{CR/IC}$
	IC	CR		
10:10	13.4	13.2	1.02	0.983
50:50	0.863	5.07	0.170	5.88
100:100	0.294	0.806	0.365	2.74
150:150	0.246	0.591	0.416	2.40
200:200	0.166	0.362	0.459	2.18

various initial concentrations, which were kept constant at a 1:1 concentration ratio. The obtained values of  $\alpha_{IC/CR}$  (1.02) and  $\alpha_{CR/IC}$  (0.983) are close to 1 for the 10:10 mg L<sup>-1</sup> IC/CR concentration, indicating a lack of selective adsorption of IC and CR by the nanoadsorbent. However, at the 50:50 mg L<sup>-1</sup> IC/CR concentration, the  $\alpha_{CR/IC}$  value increased to the highest value (5.88), whereas the  $\alpha_{IC/CR}$  value decreased to the lowest value (0.170). These results indicate that the MgFe<sub>2</sub>O<sub>4</sub>-NH<sub>2</sub> nanoadsorbent preferentially removes CR rather than IC at this concentration. With a further increase in the initial IC/CR concentration to 200:200 mg L<sup>-1</sup>, the  $\alpha_{CR/IC}$  value significantly dropped to 2.18, while the  $\alpha_{IC/CR}$  value slightly increased, leading to a decrease in the selective adsorption of CR by the nanoadsorbent. Interestingly, the molecular selectivity of the MgFe<sub>2</sub>O<sub>4</sub>-NH<sub>2</sub> nanoadsorbent seems to be influenced by the initial dye concentration, which is consistent with the report by Saghian and co-workers.<sup>37</sup> In the present study, although the



values of  $\alpha_{\text{CR/IC}}$  decreased with an increase in the IC/CR concentration (starting at 50:50 mg L<sup>-1</sup>), all obtained values were higher than 1.0 and higher than the  $\alpha_{\text{IC/CR}}$  values, indicating greater selectivity for CR over IC by the nano-adsorbent.

In the second set of experiments (see Figure 5), the ratios of IC/CR concentrations were varied when divided into two

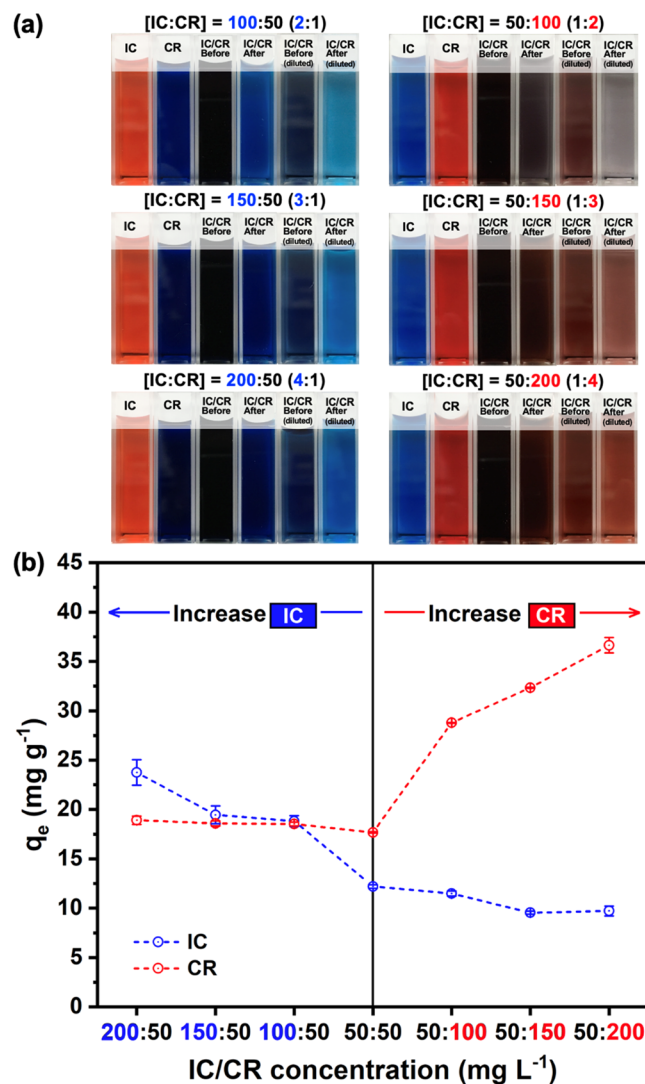


**Figure 5.** (a) Digital photos of IC/CR binary dye solutions before and after adsorption by MgFe<sub>2</sub>O<sub>4</sub>-NH<sub>2</sub> NPs. (b) Adsorption capacities of IC and CR ( $q_e$ ) on MgFe<sub>2</sub>O<sub>4</sub>-NH<sub>2</sub> NPs using various ratios of IC/CR concentrations at pH  $\sim$ 7.

subsets. In the first subset, the initial CR concentration was kept constant at 50 mg L<sup>-1</sup> and mixed with various concentrations of the IC solution (i.e., 100, 150, and 200 mg L<sup>-1</sup>) to obtain 2:1, 3:1, and 4:1 ratios of IC/CR concentrations, respectively. The complementary procedure was performed in the second subset to obtain 1:2, 1:3, and 1:4 ratios of IC/CR concentrations. The changes in the colors of the solutions during the adsorption studies and the adsorption capacities of IC and CR by the MgFe<sub>2</sub>O<sub>4</sub>-NH<sub>2</sub> NPs are illustrated in Figure 5. By keeping the CR concentration constant, the adsorption capacities of IC slightly increased with an increase in the initial IC concentration from 50 to 200 mg L<sup>-1</sup> (see Figure 5b). In contrast to the fixed IC concentration

studies, the adsorption capacities of CR significantly increased (see Figure 5b). These results indicate that although the ratios of the IC/CR concentration were varied, the MgFe<sub>2</sub>O<sub>4</sub>-NH<sub>2</sub> nanoadsorbent preferentially adsorbed CR rather than IC due to the higher adsorption capacity of CR compared to that of IC. Furthermore, the results are in good agreement with the results described in the first set.

In these studies, the molecular selectivity of the MgFe<sub>2</sub>O<sub>4</sub>-NH<sub>2</sub> nanoadsorbent could be affected by hydrogen-bonding interactions. Based on the chemical structures of CR and IC (Table 1), the -NH<sub>2</sub> groups of CR provide stronger hydrogen-bonding capacity than the -NH- group of IC.<sup>38</sup> In addition, CR bears -N=N- groups, which can form hydrogen bonds with the surface of the nanoadsorbent.<sup>28</sup> For the studies described in this section, the MgFe<sub>2</sub>O<sub>4</sub>-NH<sub>2</sub> NPs preferentially adsorbed CR rather than IC. However, the MgFe<sub>2</sub>O<sub>4</sub>-NH<sub>2</sub> nanoadsorbent was able to remove either IC or CR, indicating a lack of specificity for CR. Therefore, it is necessary to develop a new type of nanoadsorbent for the selective adsorption of Congo Red.

### 3.2. Enhanced Selective Removal of Congo Red by

#### 3.2.1. Characterization of APTES-Modified MgFe<sub>2</sub>O<sub>4</sub>@SiO<sub>2</sub> NPs.

XRD patterns of the MgFe<sub>2</sub>O<sub>4</sub> NPs after the two-step surface modification by silica and APTES are shown in Figure 6a. All diffraction patterns of the as-synthesized powders are well indexed to JCPDS card no. 88-1935, which is according to the cubic spinel MgFe<sub>2</sub>O<sub>4</sub>.<sup>12</sup> The broadening of the diffraction peak at two-theta values ranging from 20 to 30 degree can be attributed to coating with silica.<sup>39</sup> These findings suggest that silica encapsulation and APTES functionalization of MgFe<sub>2</sub>O<sub>4</sub> NPs do not influence the crystal structure of MgFe<sub>2</sub>O<sub>4</sub>. In addition, no extra diffraction peaks were found, indicating that the pure phase of MgFe<sub>2</sub>O<sub>4</sub> is maintained after the surface modification processes. FTIR spectra illustrating the functionalization of MgFe<sub>2</sub>O<sub>4</sub> NPs are provided in Figure 6b. After coating with silica, the bands at  $\sim$ 3400 and  $\sim$ 948 cm<sup>-1</sup> are assigned to the hydroxyl (O-H) stretching and bending vibration modes of the silanol (Si-OH) group, respectively.<sup>40,41</sup> In addition, the band at  $\sim$ 3400 cm<sup>-1</sup> can be attributed to adsorbed water molecules due to the detection of the O-H bending vibration of water at  $\sim$ 1630 cm<sup>-1</sup>.<sup>41,42</sup> The broad and strong band at  $\sim$ 1060 cm<sup>-1</sup> and the band at  $\sim$ 794 cm<sup>-1</sup> correspond to the stretching and bending vibration modes of the siloxane (Si-O-Si) group, respectively.<sup>43,44</sup> The vibration of metal oxides is also found at  $\sim$ 552 cm<sup>-1</sup>.<sup>44</sup> After surface functionalization by APTES, the characteristic FTIR bands detected in MgFe<sub>2</sub>O<sub>4</sub>@SiO<sub>2</sub> NPs are also observed, whereas the characteristic bands of APTES (e.g., C-H and N-H vibrations) are not readily evident. This observation is in agreement with the previous studies.<sup>45-49</sup> These studies reported that FTIR spectra of APTES-modified nanoparticles did not show the characteristic band of the APTES molecule due to the small amount of APTES species on the surface and/or the overlapping of -NH<sub>2</sub> vibration bands with those of the hydroxyl groups. In addition, Chan and Kazarian mentioned that the sensitivity of the FTIR technique is low for materials with weak absorption or when band overlapping between the minor and major components occurs.<sup>50</sup>

To clarify the nature of the surface functionalization, we used XPS to characterize the MgFe<sub>2</sub>O<sub>4</sub>@SiO<sub>2</sub> NPs before and after treatment with APTES. The corresponding survey spectra are shown in Figure 6c. All XPS spectra show the existence of

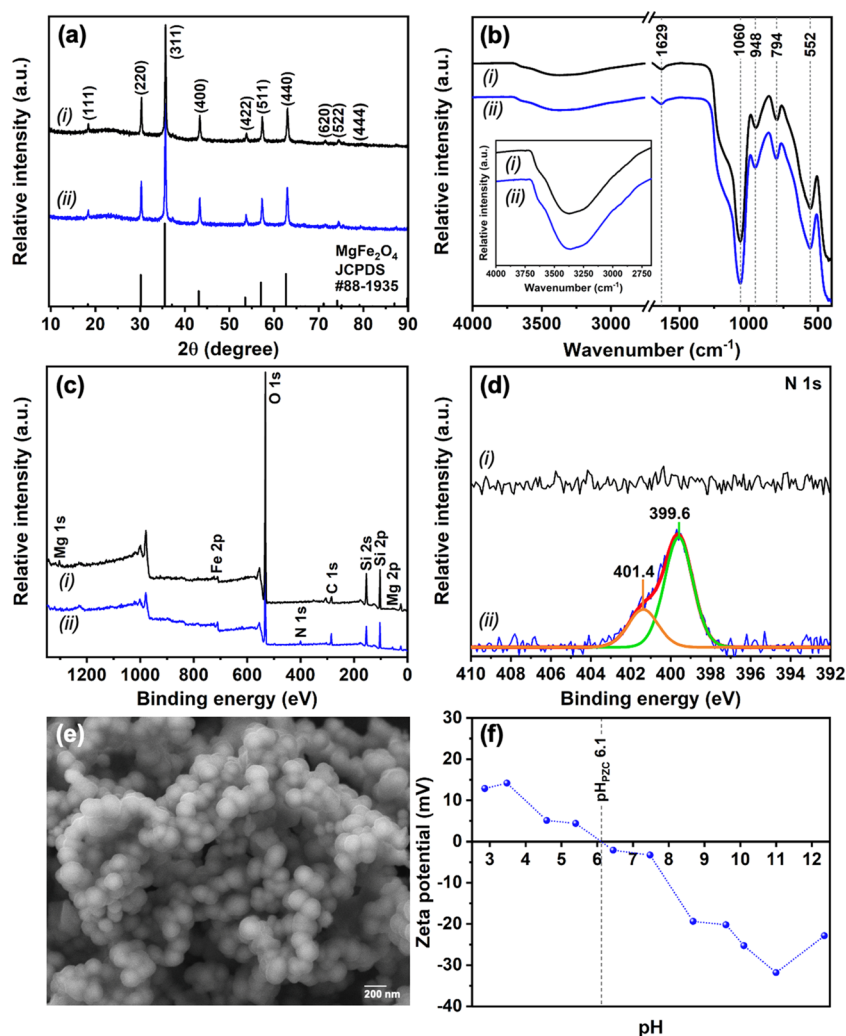


**Figure 6.** (a) XRD patterns, (b) FTIR spectra, (c) survey scan XPS spectra, and (d) high-resolution scan XPS spectra of N 1s of (i)  $\text{MgFe}_2\text{O}_4@/\text{SiO}_2$  and (ii) APTES-modified  $\text{MgFe}_2\text{O}_4@/\text{SiO}_2$  NPs. (e) SEM image and (f)  $\zeta$ -potential curve of APTES-modified  $\text{MgFe}_2\text{O}_4@/\text{SiO}_2$  NPs.

Mg, Fe, O, and Si elements, which is consistent with the chemical composition of  $\text{MgFe}_2\text{O}_4@/\text{SiO}_2$  NPs, and these results are in good agreement with the FTIR results. In addition, a signal for N was detected in the spectrum of the APTES-modified  $\text{MgFe}_2\text{O}_4@/\text{SiO}_2$  NPs, which can be attributed to the APTES molecules. Two different chemical environments of N 1s were found in the high-resolution XPS spectrum of the APTES-modified  $\text{MgFe}_2\text{O}_4@/\text{SiO}_2$  NPs (see Figure 6d). The N 1s signals at  $\sim 399.6$  and  $\sim 401.4$  eV correspond to free amine ( $-\text{NH}_2$ ) and protonated amine ( $-\text{NH}_3^+$ ) groups, respectively.<sup>46</sup> These results support the successful surface functionalization of the  $\text{MgFe}_2\text{O}_4@/\text{SiO}_2$  NPs by APTES.

Analysis of the APTES-modified  $\text{MgFe}_2\text{O}_4@/\text{SiO}_2$  NPs by SEM (see Figure 6e) reveals spherical nanoparticles with smooth surfaces, similar to the pristine  $\text{MgFe}_2\text{O}_4@/\text{SiO}_2$  NPs reported in a previous study.<sup>21</sup> The  $\zeta$ -potential was also measured to explore the surface charge properties of the APTES-modified  $\text{MgFe}_2\text{O}_4@/\text{SiO}_2$  nanoadsorbent at pH values ranging from  $\sim 3$  to  $\sim 12$ . Estimated from the  $\zeta$ -potential curve (see Figure 6f), the pH at the point of zero charge ( $\text{pH}_{\text{PZC}}$ ) of the APTES-modified  $\text{MgFe}_2\text{O}_4@/\text{SiO}_2$  NPs is  $\sim 6.1$ . The obtained  $\text{pH}_{\text{PZC}}$  value is lower than the  $\text{pK}_a$  of the propylamine surface group ( $\sim 10.6$ ), which can be attributed to the

negatively charged surface of silica.<sup>51</sup> However, the existence of APTES moieties on the surfaces leads to an increase in  $\text{pH}_{\text{PZC}}$  for the APTES-modified  $\text{MgFe}_2\text{O}_4@/\text{SiO}_2$  NPs when compared to that for the  $\text{MgFe}_2\text{O}_4@/\text{SiO}_2$  NPs ( $\sim 4.9$ ).<sup>21</sup> With regard to the characterization results obtained from XRD, FTIR, XPS, SEM, and  $\zeta$ -potential analysis, we conclude that APTES-modified  $\text{MgFe}_2\text{O}_4@/\text{SiO}_2$  NPs were successfully obtained in this study.

The magnetism of the APTES-modified  $\text{MgFe}_2\text{O}_4@/\text{SiO}_2$  NPs was examined by monitoring the response of the NPs to an external magnet in efforts to separate the nanoadsorbent from the solution. These studies found that the nanoadsorbent was rapidly separated from the solution within a few minutes (see Figure 7), indicating excellent magnetic response. In addition, the facile separation of the magnetic nanoadsorbent gives a convenient platform for reusability/sustainability.

**3.2.2. Selectivity of APTES-Modified  $\text{MgFe}_2\text{O}_4@/\text{SiO}_2$  NPs in Single-Component and Binary Dye Systems.** The as-synthesized APTES-modified  $\text{MgFe}_2\text{O}_4@/\text{SiO}_2$  NPs were utilized to investigate the selective removal of CR from both single-component and binary dye solutions. In these studies, the adsorption of dyes was investigated using  $30 \text{ mg L}^{-1}$  dye solution at  $\text{pH} \sim 6$ . The initial solution  $\text{pH} \sim 6$  was selected from the  $\zeta$ -potential curve (Figure 6f). The dye concentration

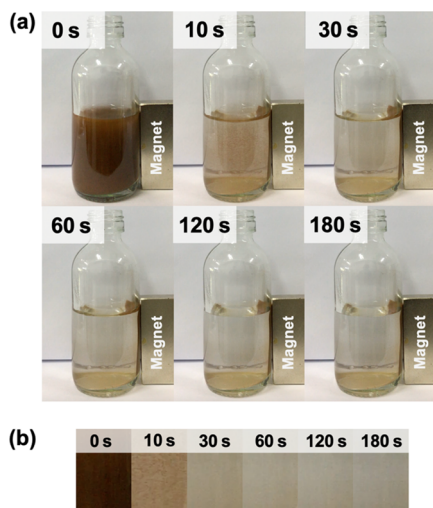


**Figure 7.** (a) Full-scale and (b) magnified digital photos of the magnetic separation over time of the APTES-modified  $\text{MgFe}_2\text{O}_4@\text{SiO}_2$  NPs.

( $30 \text{ mg L}^{-1}$ ) was selected according to the study on the effect of initial concentration of CR solution on CR adsorption, as shown in Figure S4. The removal efficiency for CR shows no significant change with an increase in CR concentration from 10 to  $30 \text{ mg L}^{-1}$  and then decreases with a further increase in CR concentration. Figure 8a shows the colors of the solutions and UV-vis spectra of the single-component dye solutions

before and after the adsorption processes. The color of the IC solution slightly faded with a small decrease in the intensity of the UV-vis absorption band of IC. In contrast, the CR solution changed from red to colorless, and the intensity of the CR absorption band decreased dramatically. The removal efficiencies for IC and CR in the single-component dye solutions were  $\sim 6$  and  $\sim 95\%$ , respectively (see Figure 8a). Interestingly, the APTES-modified  $\text{MgFe}_2\text{O}_4@\text{SiO}_2$  NPs preferentially adsorb CR rather than IC as demonstrated by the large difference in the removal efficiencies for IC and CR.

To investigate further the highly selective removal of CR by the APTES-modified  $\text{MgFe}_2\text{O}_4@\text{SiO}_2$  nanoadsorbent, we tested binary IC/CR dye systems. In Figure 8b, the color of the IC/CR solution turned blue after the adsorption process. The UV-vis absorption band for IC was largely unchanged, whereas the intensity of the CR band was strongly reduced, corresponding to  $\sim 0$  and  $\sim 94\%$  removal efficiencies for IC and CR, respectively. From the results, we conclude that APTES-modified  $\text{MgFe}_2\text{O}_4@\text{SiO}_2$  NPs show enhanced selective removal of CR compared to  $\text{MgFe}_2\text{O}_4-\text{NH}_2$  NPs.

The highly selective adsorption of CR by APTES-modified  $\text{MgFe}_2\text{O}_4@\text{SiO}_2$  NPs can be rationalized by the synergistic interplay between the adsorbent and the adsorbate. We believe that the surfaces of APTES-modified  $\text{MgFe}_2\text{O}_4@\text{SiO}_2$  NPs comprise the amine ( $-\text{NH}_2$ ) and hydroxyl ( $-\text{OH}$ ) groups, which originate from the immobilized-APTES molecules and silica surfaces, respectively. The interaction between the CR molecules and the mixture of functional groups on the nanoadsorbent surfaces can be modulated by the electrostatic

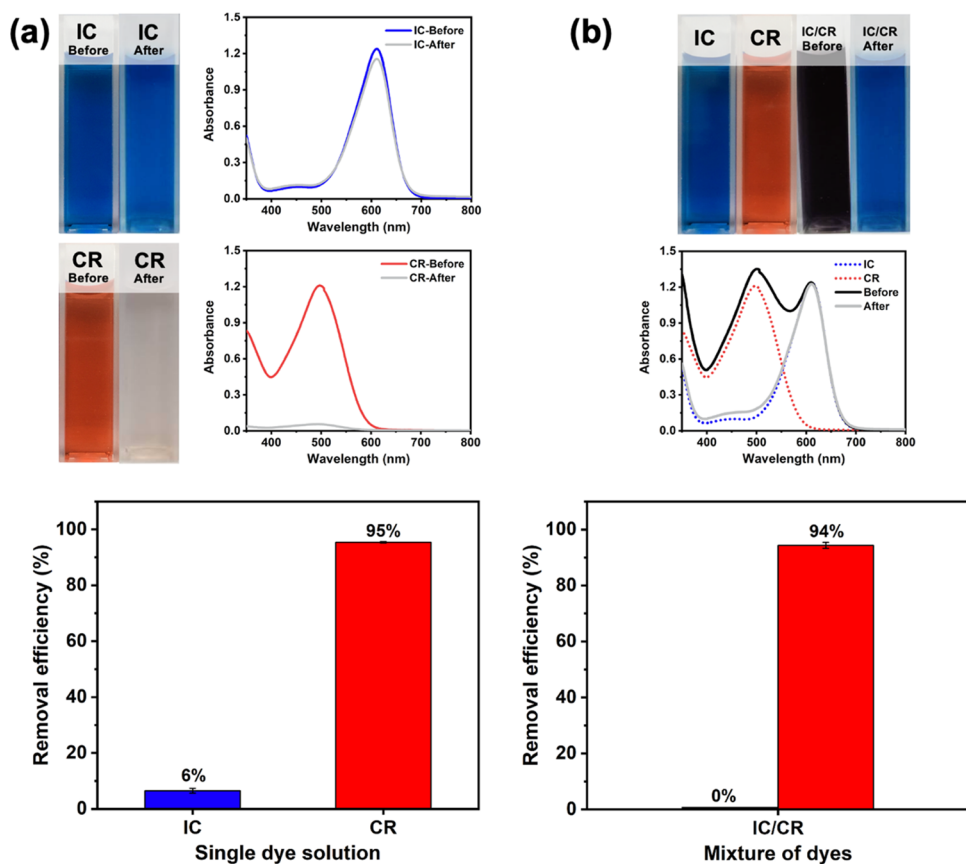


**Figure 8.** Digital photos and UV-vis spectra of (a) single-component and (b) binary dye solution systems before and after adsorption by APTES-modified  $\text{MgFe}_2\text{O}_4@\text{SiO}_2$  NPs, along with the relative removal efficiencies for the dyes at  $\text{pH} \sim 6$ .



attraction between the protonated amine groups of the nanoadsorbent and the polar functional groups of the CR molecules (i.e., amine, azo, and sulfonate groups). Even though the IC molecules also possess sulfonate groups, the adsorption results indicate that the APTES-modified  $\text{MgFe}_2\text{O}_4@/\text{SiO}_2$  nanoadsorbent does not preferably adsorb IC. From Table 1, the CR molecules are composed of two of each of the following functional groups:  $-\text{NH}_2$ ,  $-\text{N}=\text{N}-$ , and  $-\text{SO}_3^-$ , whereas IC possesses only two  $-\text{SO}_3^-$  groups. Consequently, the enhanced adsorption of CR by the nanoadsorbent is likely driven by two types of interactions as follows: (1) the dipole–dipole hydrogen-bonding (H-bonding) interactions between  $-\text{NH}_2$  or  $-\text{N}=\text{N}-$  groups of the CR molecules and the  $-\text{OH}$  groups of the adsorbent surface and (2) Yoshida H-bonding interactions between the aromatic ring of the CR molecules and the  $-\text{OH}$  groups of the adsorbent surface.<sup>28,38,52</sup>

In separate studies, we undertook computational simulations to explore the basis for the selective adsorption of CR. The net polarity of the IC and CR molecules, namely, the dipole moment ( $\mu$ ), was approximated from the optimized electronic structure of the molecule, as given in Figure S5 and Table S1. The calculated dipole moment of CR is markedly higher than that of IC, which is consistent with the high chemical reactivity of the CR molecules.<sup>27</sup> In addition, the atomic charges of N of dyes obtained from natural bond orbitals (NBO) analysis are given in Table S2. The atomic charges of N attributed to free amine groups of CR are more negative than that of pyrrole N of IC. These results thus provide additional support to our hypothesis of enhanced intermolecular interactions leading to stronger dipole–dipole H-bonding interactions between the CR molecules and the adsorbent surface.

**3.2.3. Reusability Test for CR Removal by APTES-Modified  $\text{MgFe}_2\text{O}_4@/\text{SiO}_2$  NPs.** In addition to efficient selective removal of CR, the reusability of APTES-modified  $\text{MgFe}_2\text{O}_4@/\text{SiO}_2$  NPs for CR removal was studied. The adsorption–desorption studies of CR by the nanoadsorbent for five cycles are shown in Figure 9. High removal efficiencies for CR (~98%) were

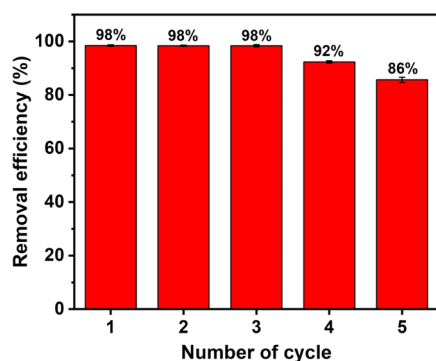


**Figure 9.** Reusability of APTES-modified  $\text{MgFe}_2\text{O}_4@/\text{SiO}_2$  NPs for Congo Red removal.

obtained in the first three cycles, which then decreased to ~92% in the fourth cycle. After the fifth cycle, the removal efficiency for CR still remained high at ~86%. Generally, the APTES-modified  $\text{MgFe}_2\text{O}_4@/\text{SiO}_2$  nanoadsorbent provides an excellent selective and reusable/sustainable system for CR removal.

## 4. CONCLUSIONS

Amine-functionalized magnesium ferrite nanoparticles ( $\text{MgFe}_2\text{O}_4-\text{NH}_2$  NPs) synthesized by our research group were used as nanoadsorbents for the adsorption of various types of organic dyes (i.e., cationic, neutral, and anionic dyes). The results demonstrated that the anionic dyes, especially IC (>90%) and CR (>90%), were removed by  $\text{MgFe}_2\text{O}_4-\text{NH}_2$  NPs from single-component and binary mixtures of dye solutions. In addition, studies of the competitive adsorption between IC and CR indicated that the  $\text{MgFe}_2\text{O}_4-\text{NH}_2$  NPs preferentially adsorbed CR (separation factor = 5.88) over IC (separation factor = 0.170) in IC/CR binary solutions. Interestingly, the selective removal of CR by  $\text{MgFe}_2\text{O}_4-\text{NH}_2$  NPs depended on the initial dye concentrations in the IC/CR binary solutions. However, the  $\text{MgFe}_2\text{O}_4-\text{NH}_2$  NPs were able to remove both IC and CR dyes, indicating a low selectivity by the nanoadsorbent. The surface of the  $\text{MgFe}_2\text{O}_4-\text{NH}_2$  NPs was further modified to achieve selective removal of CR. The surface modification was performed using two steps: (1) coating the  $\text{MgFe}_2\text{O}_4-\text{NH}_2$  NPs with silica to afford  $\text{MgFe}_2\text{O}_4@/\text{SiO}_2$  NPs and (2) surface functionalization of the  $\text{MgFe}_2\text{O}_4@/\text{SiO}_2$  NPs by 3-aminopropyltriethoxysilane (APTES) to obtain APTES-modified  $\text{MgFe}_2\text{O}_4@/\text{SiO}_2$  NPs. Characterization by XRD, FTIR, XPS, SEM, and  $\zeta$ -potential analysis confirmed the successful synthesis of the APTES-modified  $\text{MgFe}_2\text{O}_4@/\text{SiO}_2$  NPs. Adsorption studies showed that the APTES-modified  $\text{MgFe}_2\text{O}_4@/\text{SiO}_2$  nanoadsorbent provided highly selective removal of CR rather than IC in both single-component and binary mixtures of dye solutions. The enhanced selective removal of CR by the APTES-modified  $\text{MgFe}_2\text{O}_4@/\text{SiO}_2$  NPs was rationalized on the basis of the following: (1) the mixture of polar functional groups (i.e.,  $-\text{OH}$  and  $-\text{NH}_2$ ) on the surface of the nanoadsorbent, (2) the chemical nature of the dye molecules (i.e., molecular charge and functional groups), and (3) synergistic effects of the adsorption mechanism (i.e., electrostatic and hydrogen-bonding interactions). On the whole, the APTES-modified  $\text{MgFe}_2\text{O}_4@/\text{SiO}_2$  NPs offer several attractive characteristics (i.e., high performance, excellent selectivity, facile and rapid magnetic separation, and good reusability) for the removal/remediation of CR from polluted waters.

## ■ ASSOCIATED CONTENT

### Supporting Information

The Supporting Information is available free of charge at <https://pubs.acs.org/doi/10.1021/acsnm.1c01743>.

Synthesis of amine-functionalized magnesium ferrite nanoparticles; digital photos and UV–vis spectra of dyes in single-component solution systems of dyes before and after adsorption; chemical structures of NR and MO; relative removal efficiencies of dyes in cationic/cationic and cationic/neutral binary dye solutions; effect of initial concentration of the CR solution on the removal of CR by APTES-modified  $\text{MgFe}_2\text{O}_4@/\text{SiO}_2$  NPs; and computational simulations of the dipole moments and nitrogen atomic charges of IC and CR dyes (PDF)

## ■ AUTHOR INFORMATION

### Corresponding Author

Laongnuan Srisombat – Department of Chemistry, Faculty of Science and Center of Excellence in Materials Science and

Technology, Chiang Mai University, Chiang Mai 50200, Thailand; [orcid.org/0000-0003-3886-2637](https://orcid.org/0000-0003-3886-2637);  
Email: laongnuan.sri@cmu.ac.th

## Authors

**Supawitch Hoijang** – Graduate School, Chiang Mai University, Chiang Mai 50200, Thailand; Department of Chemistry, Faculty of Science, Chiang Mai University, Chiang Mai 50200, Thailand

**Tanapong Kunakham** – Department of Chemistry, Faculty of Science, Chiang Mai University, Chiang Mai 50200, Thailand

**Jeeranan Nonkumwong** – National Nanotechnology Center (NANOTEC), National Science and Technology Development Agency (NSTDA), Pathum Thani 12120, Thailand

**Kajornsak Faungnawakij** – National Nanotechnology Center (NANOTEC), National Science and Technology Development Agency (NSTDA), Pathum Thani 12120, Thailand; [orcid.org/0000-0002-4724-0613](https://orcid.org/0000-0002-4724-0613)

**Supon Ananta** – Department of Physics and Materials Science, Faculty of Science and Center of Excellence in Materials Science and Technology, Chiang Mai University, Chiang Mai 50200, Thailand

**Piyarat Nimmanpipug** – Department of Chemistry, Faculty of Science, Chiang Mai University, Chiang Mai 50200, Thailand

**T. Randall Lee** – Department of Chemistry and the Texas Center for Superconductivity, University of Houston, Houston, Texas 77204-5003, United States; [orcid.org/0000-0001-9584-8861](https://orcid.org/0000-0001-9584-8861)

Complete contact information is available at:  
<https://pubs.acs.org/10.1021/acsnm.1c01743>

## Notes

The authors declare no competing financial interest.

## ACKNOWLEDGMENTS

This research work was supported by the Basic Research Fund, Thailand Science Research and Innovation (TSRI), Chiang Mai University. The authors also acknowledge partial support from Chiang Mai University. S.H. is grateful to the Development and Promotion of Science and Technology Talents (DPST) scholarship for Ph.D. fellowship. T.R.L. acknowledges support from the US Air Force Office of Scientific Research (FA9550-20-1-0349; 20RT0302), Robert A. Welch Foundation (Grant No. E-1320), and Texas Center for Superconductivity at the University of Houston.

## REFERENCES

- (1) Mashkoo, F.; Nasar, A. Magsorbents: Potential Candidates in Wastewater Treatment T—A Review on the Removal of Methylene Blue Dye. *J. Magn. Magn. Mater.* **2020**, *500*, No. 166408.
- (2) Kumar, M.; Dosanjh, H. S.; Sonika, C.; Singh, J.; Monir, K.; Singh, H. Review on Magnetic Nanoferrites and Their Composites as Alternatives in Wastewater Treatment: Synthesis, Modifications and Applications. *Environ. Sci.: Wat. Res. Technol.* **2020**, *6*, 491–514.
- (3) Katheresan, V.; Kansedo, J.; Lau, S. Y. Efficiency of Various Recent Wastewater Dye Removal Methods: A Review. *J. Environ. Chem. Eng.* **2018**, *6*, 4676–4697.
- (4) Feng, M.; Yu, S.; Wu, P.; Wang, Z.; Liu, S.; Fu, J. Rapid, High-Efficient and Selective Removal of Cationic Dyes from Wastewater Using Hollow Polydopamine Microcapsules: Isotherm, Kinetics,

Thermodynamics and Mechanism. *Appl. Surf. Sci.* **2021**, *542*, No. 148633.

(5) Attallah, O. A.; Al-Ghobashy, M. A.; Nebsen, M.; Salem, M. Y. Removal of Cationic and Anionic Dyes from Aqueous Solution with Magnetite/Pectin and Magnetite/Silica/Pectin Hybrid Nanocomposites: Kinetic, Isotherm and Mechanism Analysis. *RSC Adv.* **2016**, *6*, 11461–11480.

(6) Bhowmik, K. L.; Debnath, A.; Nath, R. K.; Das, S.; Chattopadhyay, K. K.; Saha, B. Synthesis and Characterization of Mixed Phase Manganese Ferrite and Hausmannite Magnetic Nanoparticle as Potential Adsorbent for Methyl Orange from Aqueous Media: Artificial Neural Network Modeling. *J. Mol. Liq.* **2016**, *219*, 1010–1022.

(7) Kefeni, K. K.; Mamba, B. B.; Msagati, T. A. M. Application of Spinel Ferrite Nanoparticles in Water and Wastewater Treatment: A Review. *Sep. Purif. Technol.* **2017**, *188*, 399–422.

(8) Singh, N. B.; Nagpal, G.; Agrawal, S.; Rachna. Water Purification by Using Adsorbents: A Review. *Environ. Technol. Innovation* **2018**, *11*, 187–240.

(9) Bose, S.; Kumar Tripathy, B.; Debnath, A.; Kumar, M. Boosted Sono-Oxidative Catalytic Degradation of Brilliant Green Dye by Magnetic MgFe<sub>2</sub>O<sub>4</sub> Catalyst: Degradation Mechanism, Assessment of Bio-Toxicity and Cost Analysis. *Ultrason. Sonochem.* **2021**, *75*, No. 105592.

(10) Nonkumwong, J.; Pakawanit, P.; Wipatanawin, A.; Jantaratana, P.; Ananta, S.; Srisombat, L. Synthesis and Cytotoxicity Study of Magnesium Ferrite-Gold Core-Shell Nanoparticles. *Mater. Sci. Eng. C* **2016**, *61*, 123–132.

(11) Wei, W.; Lu, R.; Xie, H.; Zhang, Y.; Bai, X.; Gu, L.; Da, R.; Liu, X. Selective Adsorption and Separation of Dyes from an Aqueous Solution on Organic–Inorganic Hybrid Cyclomatrix Polyphosphazene Submicro-Spheres. *J. Mater. Chem. A* **2015**, *3*, 4314–4322.

(12) Zhang, P.; Yin, J.; Jiang, X. Hyperbranched Poly(ether amine)(hPEA)/poly(vinyl alcohol) (PVA) Interpenetrating Network (IPN) for Selective Adsorption and Separation of Guest Homologues. *Langmuir* **2014**, *30*, 14597–14605.

(13) Qin, Y.; Wang, L.; Zhao, C.; Chen, D.; Ma, Y.; Yang, W. Ammonium-Functionalized Hollow Polymer Particles as a pH-Responsive Adsorbent for Selective Removal of Acid Dye. *ACS Appl. Mater. Interfaces* **2016**, *8*, 16690–16698.

(14) Chen, F.; Zhao, E.; Kim, T.; Wang, J.; Hableel, G.; Reardon, P. J. T.; Ananthakrishnan, S. J.; Wang, T.; Arconada-Alvarez, S. J.; Knowles, J. C.; Jakerst, J. V. Organosilica Nanoparticles with an Intrinsic Secondary Amine: An Efficient and Reusable Adsorbent for Dyes. *ACS Appl. Mater. Interfaces* **2017**, *9*, 15566–15576.

(15) Nonkumwong, J.; Ananta, S.; Srisombat, L. Effective Removal of Lead(II) from Wastewater by Amine-Functionalized Magnesium Ferrite Nanoparticles. *RSC Adv.* **2016**, *6*, 47382–47393.

(16) Aoopngan, C.; Nonkumwong, J.; Phumying, S.; Promjantuek, W.; Maensiri, S.; Noisa, P.; Pinitsoontorn, S.; Ananta, S.; Srisombat, L. Amine-Functionalized and Hydroxyl-Functionalized Magnesium Ferrite Nanoparticles for Congo Red Adsorption. *ACS Appl. Nano Mater.* **2019**, *2*, 5329–5341.

(17) Hoijang, S.; Nonkumwong, J.; Singhana, B.; Wangkarn, S.; Ananta, S.; Srisombat, L. Adsorption of 2,4-Dichlorophenoxyacetic Acid by Magnesium Ferrite Magnetic Nanoparticles Modified with Amine Functional Groups. *Chiang Mai J. Sci.* **2020**, *47*, 137–146.

(18) Karade, V. C.; Sharma, A.; Dhavale, R. P.; Shingte, S. R.; Patil, P. S.; Kim, J. H.; Zahn, D. R. T.; Chougale, A. D.; Salvan, G.; Patil, P. B.; et al. APTES Monolayer Coverage on Self-Assembled Magnetic Nanospheres for Controlled Release of Anticancer Drug Nintedanib. *Sci. Rep.* **2021**, *11*, No. 5674.

(19) Bondarenko, L.; Illés, E.; Tombác, E.; Dzhardimalieva, G.; Golubeva, N.; Tushavina, O.; Adachi, Y.; Kydralieva, K. Fabrication, Microstructure and Colloidal Stability of Humic Acids Loaded Fe<sub>3</sub>O<sub>4</sub>/APTES Nanosorbents for Environmental Applications. *Nanomaterials* **2021**, *11*, No. 1418.

(20) Wallace, R. M. Analysis of Absorption Spectra of Multi-component Systems. *J. Phys. Chem. A* **1960**, *64*, 899–901.

- (21) Hoiyang, S.; Wangkarn, S.; Ieamviteevanich, P.; Pinitsoontorn, S.; Ananta, S.; Lee, T. R.; Srisombat, L. Silica-Coated Magnesium Ferrite Nanoadsorbent for Selective Removal of Methylene Blue. *Colloids Surf., A* **2020**, *606*, No. 125483.
- (22) Kim, J. H.; Chung, H. W.; Lee, T. R. Preparation and Characterization of Palladium Shells with Gold and Silica Cores. *Chem. Mater.* **2006**, *18*, 4115–4120.
- (23) Zou, W. H.; Bai, H. J.; Gao, S. P. Competitive Adsorption of Neutral Red and  $\text{Cu}^{2+}$  onto Pyrolytic Char: Isotherm and Kinetic Study. *J. Chem. Eng. Data* **2012**, *57*, 2792–2801.
- (24) Sarkar, N.; Sahoo, G.; Das, R.; Swain, S. K. Three-Dimensional Rice Straw-Structured Magnetic Nanoclay-Decorated Tripolymeric Nanohydrogels as Superadsorbent of Dye Pollutants. *ACS Appl. Nano Mater.* **2018**, *1*, 1188–1203.
- (25) Zhang, W.; Zhang, R. Z.; Huang, Y. Q.; Yang, J. M. Effect of the Synergetic Interplay Between the Electrostatic Interactions, Size of the Dye Molecules, and Adsorption Sites of MIL-101(Cr) on the Adsorption of Organic Dyes from Aqueous Solutions. *Cryst. Growth Des.* **2018**, *18*, 7533–7540.
- (26) Lillie, R. D.; Conn, H. J.; Stotz, E. H.; Emmel, V. M. H. J. *Conn's Biological Stains: A Handbook on the Nature and Uses of the Dyes Employed in the Biological Laboratory*, 9th ed.; Williams and Wilkins: Baltimore, MD, 1977; p 378.
- (27) Regti, A.; Ben El Ayouchia, H.; Laamari, M. R.; Stiriba, S. E.; Anane, H.; El Haddad, M. Experimental and Theoretical Study Using DFT Method for the Competitive Adsorption of Two Cationic Dyes from Wastewaters. *Appl. Surf. Sci.* **2016**, *390*, 311–319.
- (28) Liu, X. Y.; An, S.; Wang, Y. J.; Yang, Q.; Zhang, L. Rapid Selective Separation and Recovery of a Specific Target Dye from Mixture Consisted of Different Dyes by Magnetic Ca-Ferrites Nanoparticles. *Chem. Eng. J.* **2015**, *262*, 517–526.
- (29) Middea, A.; Spinelli, L. S.; Souza, F. G., Jr; Neumann, R.; Fernandes, T. L. A. P.; Gomes, O. D. F. M. Preparation and Characterization of an Organo-Palygorskite- $\text{Fe}_3\text{O}_4$  Nanomaterial for Removal of Anionic Dyes from Wastewater. *Appl. Clay Sci.* **2017**, *139*, 45–53.
- (30) Gamoudi, S.; Srasra, E. Adsorption of Organic Dyes by HDPY<sup>+</sup>-Modified Clay: Effect of Molecular Structure on the Adsorption. *J. Mol. Struct.* **2019**, *1193*, 522–531.
- (31) Yang, J. M.; Zhang, W.; Zhang, R. Z.; Tong, M. X. Modulation of the Driving Forces for Adsorption on MIL-101 Analogues by Decoration with Sulfonic Acid Functional Groups: Superior Selective Adsorption of Hazardous Anionic Dyes. *Dalton Trans.* **2020**, *49*, 6651–6660.
- (32) Chatterjee, S.; Guha, N.; Krishnan, S.; Singh, A. K.; Mathur, P.; Rai, D. K. Selective and Recyclable Congo Red Dye Adsorption by Spherical  $\text{Fe}_3\text{O}_4$  Nanoparticles Functionalized with 1,2,4,5-Benzene-tetracarboxylic Acid. *Sci. Rep.* **2020**, *10*, No. 111.
- (33) Jia, Y. H.; Ding, L.; Ren, P. Y.; Zhong, M. Y.; Ma, J. Y.; Fan, X. R. Performances and Mechanism of Methyl Orange and Congo Red Adsorbed on the Magnetic Ion-Exchange Resin. *J. Chem. Eng. Data* **2020**, *65*, 725–736.
- (34) Liu, H. C.; Chen, L. G.; Ding, J. Adsorption Behavior of Magnetic Amino-Functionalized Metal-Organic Framework for Cationic and Anionic Dyes from Aqueous Solution. *RSC Adv.* **2016**, *6*, 48884–48895.
- (35) Pan, J.; Zhou, L.; Chen, H.; Liu, X.; Hong, C.; Chen, D.; Pan, B. Mechanistically Understanding Adsorption of Methyl Orange, Indigo Carmine, and Methylene Blue onto Ionic/Nonionic Polystyrene Adsorbents. *J. Hazard. Mater.* **2021**, *418*, No. 126300.
- (36) Kyzas, G. Z.; Bikiaris, D. N.; Lazaridis, N. K. Selective Separation of Basic and Reactive Dyes by Molecularly Imprinted Polymers (MIPs). *Chem. Eng. J.* **2009**, *149*, 263–272.
- (37) Saghian, M.; Dehghanpour, S.; Sharbatdaran, M. Unique and Efficient Adsorbents for Highly Selective and Reverse Adsorption and Separation of Dyes via the Introduction of  $\text{SO}_3\text{H}$  Functional Groups into a Metal-Organic Framework. *RSC Adv.* **2020**, *10*, 9369–9377.
- (38) Li, N.; Dang, H.; Chang, Z.; Zhao, X.; Zhang, M.; Li, W.; Zhou, H.; Sun, C. Synthesis of Uniformly Distributed Magnesium Oxide Micro-/Nanostructured Materials with Deep Eutectic Solvent for Dye Adsorption. *J. Alloys Compd.* **2019**, *808*, No. 151571.
- (39) Sun, L.; Li, Y. X.; Sun, M. D.; Wang, H. G.; Xu, S. F.; Zhang, C. Q.; Yang, Q. B. Porphyrin-Functionalized  $\text{Fe}_3\text{O}_4@/\text{SiO}_2$  Core/Shell Magnetic Colorimetric Material for Detection, Adsorption and Removal of  $\text{Hg}^{2+}$  in Aqueous Solution. *New J. Chem.* **2011**, *35*, 2697–2704.
- (40) Zhang, S. X.; Zhang, Y. Y.; Liu, J. S.; Xu, Q.; Xiao, H. Q.; Wang, X. Y.; Xu, H.; Zhou, J. Thiol Modified  $\text{Fe}_3\text{O}_4@/\text{SiO}_2$  as a Robust, High Effective, and Recycling Magnetic Sorbent for Mercury Removal. *Chem. Eng. J.* **2013**, *226*, 30–38.
- (41) Post, P.; Wurlitzer, L.; Maus-Friedrichs, W.; Weber, A. P. Characterization and Applications of Nanoparticles Modified In-Flight with Silica or Silica-Organic Coatings. *Nanomaterials* **2018**, *8*, No. 530.
- (42) Jiang, T.; Kuila, T.; Kim, N. H.; Lee, J. H. Effects of Surface-Modified Silica Nanoparticles Attached Graphene Oxide Using Isocyanate-Terminated Flexible Polymer Chains on the Mechanical Properties of Epoxy Composites. *J. Mater. Chem. A* **2014**, *2*, 10557–10567.
- (43) Javaheri, F.; Hassanajili, S. Synthesis of  $\text{Fe}_3\text{O}_4@/\text{SiO}_2@/\text{MPS}@/\text{P4VP}$  Nanoparticles for Nitrate Removal from Aqueous Solutions. *J. Appl. Polym. Sci.* **2016**, *133*, No. 44330.
- (44) Roto, R.; Yusran, Y.; Kuncaka, A. Magnetic Adsorbent of  $\text{Fe}_3\text{O}_4@/\text{SiO}_2$  Core-Shell Nanoparticles Modified with Thiol Group for Chloroauric Ion Adsorption. *Appl. Surf. Sci.* **2016**, *377*, 30–36.
- (45) Berktaş, I.; Ghafar, A. N.; Fontana, P.; Caputcu, A.; Menciloglu, Y.; Okan, B. S. Facile Synthesis of Graphene from Waste Tire/Silica Hybrid Additives and Optimization Study for the Fabrication of Thermally Enhanced Cement Grouts. *Molecules* **2020**, *25*, No. 886.
- (46) Obaidullah, M.; Bahadur, N. M.; Furusawa, T.; Sato, M.; Sakuma, H.; Suzuki, N. Microwave Assisted Rapid Synthesis of  $\text{Fe}_2\text{O}_3@/\text{SiO}_2$  Core-Shell Nanocomposite for the Persistence of Magnetic Property at High Temperature. *Colloids Surf., A* **2019**, *572*, 138–146.
- (47) Sodipo, B. K.; Aziz, A. A. One Minute Synthesis of Amino-Silane Functionalized Superparamagnetic Iron Oxide Nanoparticles by Sonochemical Method. *Ultrason. Sonochem.* **2018**, *40*, 837–840.
- (48) Sodipo, B. K.; Aziz, A. A. A Sonochemical Approach to the Direct Surface Functionalization of Superparamagnetic Iron Oxide Nanoparticles with (3-Aminopropyl)triethoxysilane. *Beilstein J. Nanotechnol.* **2014**, *5*, 1472–1476.
- (49) Ataee-Esfahani, H.; Nemoto, Y.; Wang, L.; Yamauchi, Y. Rational Synthesis of Pt Spheres with Hollow Interior and Nanosponge Shell Using Silica Particles as Template. *Chem. Commun.* **2011**, *47*, 3885–3887.
- (50) Chan, K. L. A.; Kazarian, S. G. Detection of Trace Materials with Fourier Transform Infrared Spectroscopy Using a Multi-Channel Detector. *Analyst* **2006**, *131*, 126–131.
- (51) Nguyen, Q. X.; Belgard, T. G.; Taylor, J. J.; Murthy, V. S.; Halas, N. J.; Wong, M. S. Water-Phase Synthesis of Cationic Silica/Polyamine Nanoparticles. *Chem. Mater.* **2012**, *24*, 1426–1433.
- (52) Ghorai, S.; Sarkar, A.; Raoufi, M.; Panda, A. B.; Schonherr, H.; Pal, S. Enhanced Removal of Methylene Blue and Methyl Violet Dyes from Aqueous Solution Using a Nanocomposite of Hydrolyzed Polyacrylamide Grafted Xanthan Gum and Incorporated Nanosilica. *ACS Appl. Mater. Interfaces* **2014**, *6*, 4766–4777.